Available online at www.sciencedirect.com
ScienceDirect
Trans. Nonferrous Met. Soc. China 34(2024) 4049−4062
Transactions of Nonferrous Metals Society of China
www.tnmsc.cn

Influence of tartrate on leaching interface of low-grade polymetallic complex chalcopyrite ore

Xin-Jie LIU, Ya-long LIAO, Qing-feng LIU, Min WU

Faculty of Metallurgical and Energy Engineering, Kunming University of Science and Technology, Kunming 650093, China

Received 25 April 2023; accepted 6 December 2023

Abstract: The leaching of Cu from low-grade polymetallic complex chalcopyrite ore (LPCCO) in acidic ferric electrolyte was increased by adding tartrate. To explain the reason resulting in this phenomenon, a systematical study about the effects of tartrate on the interfaces where reactions occurred was conducted by using electrochemical methods. The Mott−Schottky experiment results showed that whether tartrate was added or not, the initial n-type LPCCO surface transformed to the surface with a p−n junction that seriously hindered charge transfer. After adding tartrate, a shorter Debye length and higher charge carrier density were obtained, which were related to the decrease in intergranular energy barrier height by tartrate's bridging semiconductor particles. Additionally, EIS results combined with Tafel and LSV analysis revealed thin passive film and double-layer, large diffusion coefficient, and low apparent activation energy. These favorable changes in interface properties facilitated the LPCCO dissolution.

Key words: interface; chalcopyrite; passivation; semiconductor; leaching

1 Introduction

As the continuous exploitation and consumption of copper ores, poor mineral ores containing $CuFeS_2$, PbS, FeS_2, and ZnS, etc, have to be faced for utilization. For the reason that these components are mutually entangled tightly in the original ore, it is difficult to separate them by dressing process. Therefore, a large amount of low-grade polymetallic complex chalcopyrite ore (LPCCO), a typical refractory mineral ore, is produced. For effective utilization of copper resources contained in LPCCO, it is necessary and significant to research and develop effective extracting methodologies. When this kind of raw material is treated by traditional pyrometallurgical methodologies, not only the recovery rate of metal is low and the economic and technical index is not ideal, but also large amounts of greenhouse gases and harmful sulfur dioxide are emitted as well. Alternatively, hydrometallurgical process of the extracting valuable metals from an aqueous solution at low temperature or normal temperature with low energy consumption and strong environmental compatibility [1] has gradually become an efficient method to treat copper sulfide, especially LPCCO.

Leaching, one of the unit procedures in hydrometallurgical processes, is an attractive separation method of valuable metals from LPCCO. Due to the special crystal and electronic structure of chalcopyrite, a solid passive film is formed on its surface, which limits the contact and diffusion process between the leaching agent and the mineral, leading to the reduction of the leaching rate of valuable metals. Additionally, the composition of passive film is still under debate, although most speculations are related to elemental sulfur (S^0),

Corresponding author: Ya-long LIAO, Tel: +86-871-65198154, E-mail: liaoylsy@163.com
DOI: 10.1016/S1003-6326(24)66657-4

polysulfide (S_n^{2-}), metal defect sulfide, jarosite/lead jarosite [2], and secondary minerals [3]. Therefore, it has become a hot problem how to find new methods to improve the dissolution rate of chalcopyrite and extract valuable metals from chalcopyrite more efficiently.

Although the conditions of high temperature (200 °C) and high O_2 partial pressure (1.2 MPa) could achieve more than 98% leaching rate of Cu from LPCCO [4], these leaching conditions are harsh. Other attempts have been made to weaken the negative effects of the passive film during leaching of LPCCO. One of these attempts is adding additives, such as organic [5,6], Ag^+ [7] and pyrite [8]. The functions of these additives involve increasing the porosity [9], hydrophilicity [10] and conductivity of passive film by attacking or doping it, and constructing stable galvanic effects between ores.

Essentially, these additives improve the properties of leaching interfaces [11], such as structure, composition and thickness, thus enhancing the leaching rate of chalcopyrite. It was reported that natural chalcopyrite was a p-type or n-type semiconductor [12−14]. The leaching interfaces and processes will become more complex if passive species with special conducting properties are produced or deposited on the semiconductor surface. However, few systematic and comprehensive studies involving the interfaces associated with semiconductor−semiconductor and semiconductor−solution have been reported, which are closely related to the leaching behaviors of chalcopyrite and/or LPCCO. Recently, tartrate has attracted more and more attention for its outstanding performance as a catalytic additive in hydrometallurgy. It could increase the reactivity and leaching efficiency of metals from the spent batteries [15]. Additionally, tartrate ligands could promote the dissolution of metals [16] and prevent metals and passive species from accumulating on the solid surface [17,18]. As a surfactant and catalyzer, tartrate could be used as an additive for improving the extracting efficiency of lead [19,20], zinc [20], as well as gold and silver [21].

In the present work, tartrate was employed as an additive to explore the detailed information about interface/surface during the leaching of LPCCO in the acidic ferric ion electrolyte. As the reason that easier leaching of Zn and Pb from LPCCO was found, while Cu was more difficult to be leached. Therefore, only copper leaching is mentioned in the present work. Electrochemical methods, such as Mott−Schottky (M−S) measurements, Tafel polarization, electrochemical impedance spectroscopy (EIS) and linear sweep voltammetry (LSV) were utilized aiming at qualifying and quantifying the effect of tartrate on interface. The interface behaviors involving electron/charge transfer across semiconductor−semiconductor and semiconductor−liquid interfaces, molecular adsorption, diffusion, and apparent activation energy were systematically studied, and a model of p−n junction was proposed to help us have deep insights into leaching interfaces and de-passivation mechanisms. The results obtained show that tartrate is a promising additive that can improve the interface properties (such as charge carrier density and resistance of charge transfer) during leaching of LPCCO, which finally facilitate LPCCO dissolution.

2 Experimental

2.1 Characterization of raw material (LPCCO)

The raw material (LPCCO) was from a mineral enterprise in Yunnan Province of China. After wet ball milling, screening, filtering and drying, the experimental raw material with particle sizes less than 75 μm was obtained. The content of chemical elements in LPCCO was quantitatively measured by an Inductively Coupled Plasma-Atomic Emission Spectrometer (ICP-AES) (Optima−5300DV, Pekin Elmer Company, United States). As shown in Table 1, the copper content is 11.10 wt.%. The LPCCO was further characterized by X-ray diffractometer (XRD) (X'Pert Pro MPD, Panaco Analytical Instruments Company, Netherlands) combined with Optical microscopy (OM, Carl Zeiss German) and electron probe microanalysis (EPMA, JXA−8230 Japan). The results of mineral composition and relative content of LPCCO are shown in Table 2. The XRD results are shown in our previous paper [4]. Table 2 shows that FeS_2 has the highest content (45 wt.%), followed by $CuFeS_2$ (30 wt.%) which is more active

Table 1 Main element content of LPCCO (wt.%)

Cu	Fe	Zn	S	Pb	Al_2O_3	SiO_2	CaO	MgO
11.10	28.10	2.97	34.95	8.88	0.50	1.86	0.38	0.43

Table 2 Mineral composition and content of raw materials

Type	Mineralogical phase	Composition	Content/ wt.%
Oxide	Gangue	SiO_2, MgO, CaO, Al_2O_3	5.0
Sulfide	Chalcopyrite	$CuFeS_2$	30.0
	Bornite	Cu_5FeS_4	2.0
	Pyrite	FeS_2	45.0
	Galena	PbS	11.0
	Sphalerite	ZnS	5.0

than FeS_2, but less active than ZnS and PbS [8].

2.2 Leaching experiment

The leaching experiments of LPCCO were conducted in the flask (250 mL) equipped with mixer, condenser, and thermometer (Fig. 1(a)). The solution (50 mL) for extracting Cu consisted of 1 mol/L HCl and 0.1 mol/L $FeCl_3$ without or with 0.1 mol/L tartrate. The ratio of LPCCO mass to liquid volume was 1:25 g/mL. The leaching experiments were performed under atmospheric pressure at different temperatures (298−358 K) and time (1−18 h) with 400 r/min stirring speed. The Cu concentration in the solution after leaching was determined by the chemical titration and ICP-AES measure.

The concentrated hydrochloric acid (analytical reagent, 36−38 wt.%), ferric chloride hexahydrate (III) (analytical pure, >99 wt.%), L-(+) sodium tartrate dihydrate (analytical reagent, >99 wt.%) and distilled water were used to prepare the solution for extracting Cu.

2.3 Working electrode preparation

A self-made LPCCO electrode, working electrode, was made by pressing carbon paste into an L-shaped plexiglass tube with force of 50 N. The carbon paste consisted of LPCCO, graphite power and liquid paraffin oil with a mass ratio of 2:4:1.35 by mixing the components in an agate mortar and grinding for 30 min to achieve homogeneity. Graphite powder (>98%) and liquid paraffin oil were chemically pure. The Pt line was placed inside the L-shaped electrode and connected with the filled carbon paste. A rubber plug was used for blocking. The epoxy resin was employed to seal the electrode. The inner diameter of the L-shaped electrode was 5.0 mm, in which 0.35 g of the carbon paste was filled each time, and the exposed area of the electrode was 19.6 mm^2 (Fig. 1(b)).

2.4 Electrochemical measurement

The electrochemical measurements were carried out in a traditional three-electrode cylindrical battery without stirring at 318 K (Fig. 1(c)). The electrolyte (50 mL) consisted of 1 mol/L HCl and 0.1 mol/L $FeCl_3$ without or with 0.1 mol/L tartrate. The working electrode was the L-shaped electrode and the auxiliary electrode was a Pt electrode. The Ag/AgCl electrode (0.222 V vs standard hydrogen electrode) was employed as the reference electrode. The working electrode was placed with a gesture that exposed surface faced toward the auxiliary electrode, and the distance between them was 1 cm. All the electrochemical experiments were conducted by using a CHI 660 electrochemical workstation (Shanghai Chenhua Instrument Co., Ltd., China).

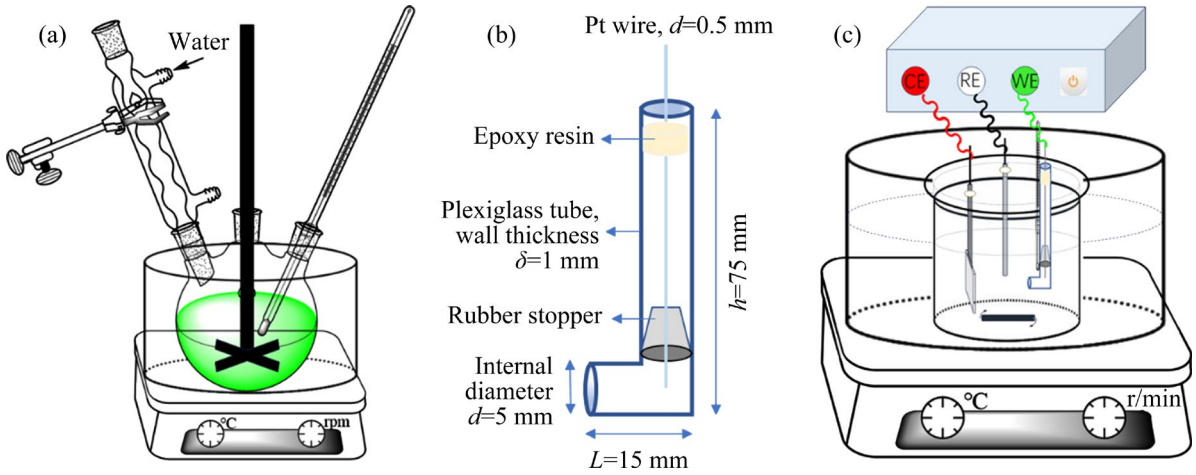

Fig. 1 Device diagram of leaching (a), working electrode (b) and electrochemistry experiment (c)

Mott–Schottky (M-S) analysis was conducted at a frequency of 1 kHz in the potential range from 0.52 to 1.24 V with an amplitude of 5 mV peak-to-peak. The Tafel curve was measured at the scanning rate (v) of 1 mV/s and fitted in the CHI 660 electrochemical workstation. The registered open circuit potential (OCP) in the case without or with tartrate was 0.602 and 0.608 V, respectively. A slightly high OCP was attributed to the decrease in the concentration of H^+ caused by the formation of tartaric acid from some tartrate, which slightly affected the initial dissolution of MgO, CaO and Al_2O_3 in LPCCO. The electrochemical impedance spectroscopy (EIS) was implemented from 100 kHz to 0.1 Hz with an amplitude of 10 mV at different potentials. Analysis of the EIS data was conducted by fitting the experimental data in the ZView software. The LSV was performed at different scanning rates and/or temperatures.

Before each electrochemical measurement, the exposed surface of the L-shaped electrode was polished with a sequence of emery paper of different grades (18, 13 and 6.5 μm) until a fresh and smooth surface was produced. Subsequently, the surface of the electrode was carefully washed with 1 mol/L HCl followed by distilled water. All the potentials reported in this work were relative to the Ag/AgCl electrode.

3 Results and discussion

3.1 Effect of tartrate on LPCCO leaching

Figure 2(a) shows the effect of leaching time (t) on the Cu extraction rates in the solution without and with 0.1 mol/L tartrate. Within 15 h, the Cu extraction rates keep increasing. When the leaching time is past 15 h, the extraction rates increase slowly due to the inhibition of passive film for both cases. When tartrate is present, the Cu extraction rate is higher than that when it is absent. Figure 2(b) shows that the increase in temperature (T) can increase the Cu extraction rate. As temperature increases in the range of 298−328 K, the Cu extraction rate increases slower than that in the range of 338−358 K for both cases. This is attributed to the fact that the energy barrier responsible for the slow copper dissolution rate is overcome. At the scope of 298 to 358 K, the case with tartrate is of high leaching rate. As shown in Fig. 2(c), as the increase in the concentration of tartrate at the scope of 0−0.10 mol/L, the Cu extraction rate increases. When the concentration of tartrate is over 0.10 mol/L, the Cu extraction rate decreases, which is attributed to the agglomeration of tartrate/tartaric molecules. The leaching experiments indicate that tartrate can facilitate Cu extraction from LPCCO.

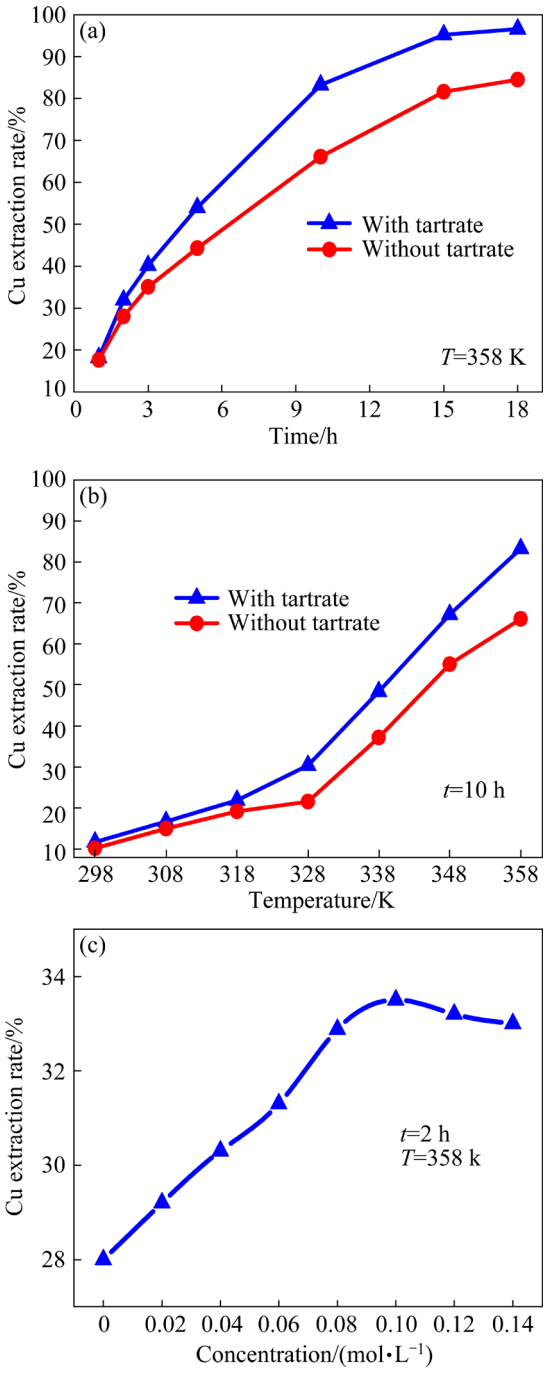

Fig. 2 Effects of leaching time (a), temperature (b) and concentration of tartrate (c) on Cu extraction rate in 1 mol/L HCl and 0.1 mol/L $FeCl_3$ solution without and with 0.1 mol/L tartrate at atmospheric pressure under 400 r/min

3.2 Analysis of interfaces

3.2.1 Interfaces concerning semiconductor

For explaining the reason why tartrate improves leaching, the analysis of LPCCO's interfaces where reaction occurs was conducted by using electrochemical methods. To get the stable electrochemical data revealing the effect of tartrate on interfaces, the electrochemical experiments were conducted at 318 K without stirring. According to the Mott−Schottky equation (Eq. (1)), the flat band potential (φ_{fb}) can be evaluated because Helmholtz layer capacitance (C_H) is 2−3 orders larger than space charge layer capacitance (C_{sc}) [22],

$$\frac{1}{C}=\frac{1}{C_H}+\frac{1}{C_{sc}}\approx\frac{1}{C_{sc}}=\left[\frac{2}{e\varepsilon\varepsilon_0 n_0}\left(E-\varphi_{fb}-\frac{kT}{e}\right)\right]^{1/2} \tag{1}$$

where C, e, ε, ε_0, n_0, E, k and T are the overall interface capacitance (F/m^2), charge of an electron (1.6×10^{-19} C), dielectric constant of the semiconductor (for chalcopyrite, ε varies from 10 to 81 [23]), vacuum permittivity of free space (8.85×10^{-12} F/m), charge carrier density (m^{-3}), applied potential (V), Boltzmann constant (1.38×10^{-23} J/K) and temperature (K), respectively. The term kT/e is 0.0274 V at 318 K.

As shown in Fig. 3(a), the values of the term $\varphi_{fb}+kT/e$ are 0.5700 and 0.5600 V, therefore, φ_{fb} is 0.5426 and 0.5326 V for the cases without and with tartrate, respectively. For both cases, φ_{fb} is lower than OCP labeled in Fig. 3(a), indicating that fresh LPCCO surface remains in the depletion state when it is contacted with the electrolyte, which is consistent with that in the literature [12]. The lower φ_{fb} when tartrate is present is possibly due to the change in potential drop across the Helmholtz layer [24], suggesting a weaker bending of energy band and less electron transfer (ET) obstacle.

In the region of 0.52−0.74 V (or 0.76 V in the case without tartrate, Fig. 3(a)), the positive slope indicates that LPCCO is an n-type semiconductor contributed by n-type semiconductor construct of $CuFeS_2$ and FeS_2 [25]. But FeS_2 is more inert than $CuFeS_2$ [8]. Compared with the slope at the scope of 0.52−0.60 V, the bigger slope at the scope of 0.60−0.68 V implies a decrease in n_0 of the surface layer [2], which is induced by the initial dissolutions of PbS, ZnS and chalcopyrite that preferentially releases Fe atom. The slopes in this region were fitted, as shown in Fig. 3(a), for

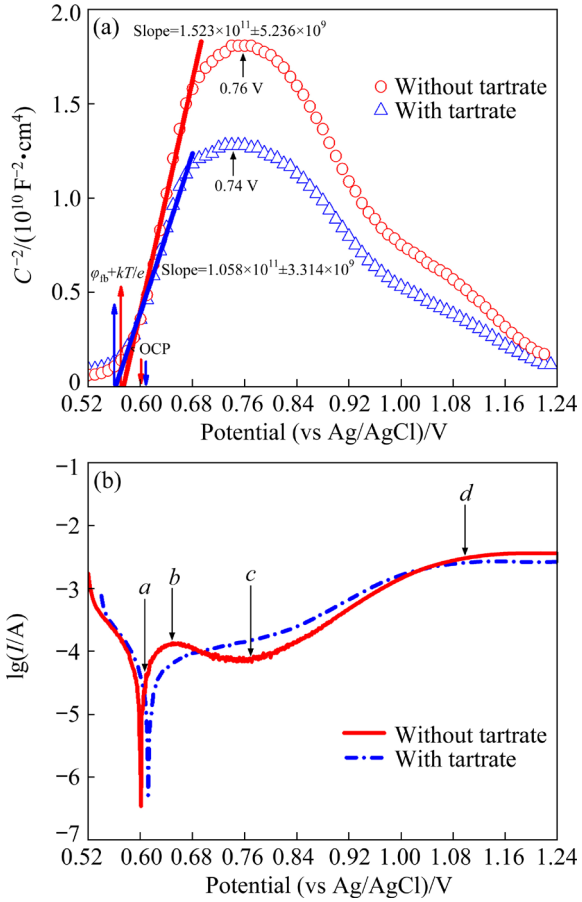

Fig. 3 Mott–Schottky plots (a) and Tafel polarization curves (b) for LPCCO electrodes at 318 K

calculating n_0. Additionally, the Debye length ($L_{D.eff}$) was also calculated by Eq. (2) [2].

$$L_{D.eff}=\left(\frac{\varepsilon\varepsilon_0 kT}{2e^2 n_0}\right)^{1/2} \tag{2}$$

The values of n_0 obtained are 1.14×10^{25} and 1.65×10^{25} m^{-3}, and $L_{D.eff}$ is 2.25 and 1.88 nm, respectively in the cases without and with tartrate by assuming the value of ε as 81 [23], and assuming that the capacitance measured by the Mott–Schottky method is very close to the C_{sc} and that the dielectric constants of all surface layers are close to that of the chalcopyrite [2]. In this work, n_0 and $L_{D.eff}$ are a little bigger than that (0.88×10^{25} m^{-3} and 0.9 nm) reported in Ref. [2], which are due to the different acid systems used. When tartrate is added, the bigger n_0 indicates a higher conductivity and reaction rate, additionally, a shorter $L_{D.eff}$ is highly desirable for faster electron-hole separation that can enhance the activity of the anode [26].

The slopes invert at 0.76 and 0.74 V respectively for the case without and with tartrate,

indicating the formation of a p-type product. This is attributed to the formation of a copper-rich, covellite-like layer mixed with S^0 induced by the preferential release of iron atoms, which is verified by XPS analysis (Fig. 4). The newborn peak at 568.5 eV in the case without and with tartrate corresponds to the typical peak of covellite (CuS) [27], indicating the formation of CuS.

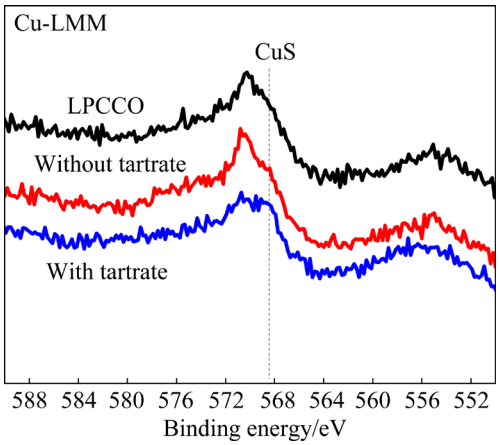

Fig. 4 Cu-LMM of LPCCO and residual solids obtained after leaching (318 K, 3 h, and 400 r/min) without and with tartrate in XPS analysis

The copper-rich, covellite-like layer was regarded as a p-type semiconductor [14]. The transformation of semiconductor on the surface will result in the rapid formation of a p−n junction, leading to the mineral transitions from resistance to diode.

As shown in Fig. 5, in the p−n junction, there is a space charge region (SCR) whose energy band is bent. However, the p−n junction is under the reverse bias, and the SCR will transform into a depletion region induced by the exhaustion of the orienteering charge carrier (Fig. 5). The depletion region will keep expanding until the diffusion-current and drift-current reach balance, and the movement of charge carriers in depletion region is obstructed. Therefore, there is a very low current in the p−n junction, as shown in Tafel polarization curves (Point *c* in Fig. 3(b)). It can be expected that the slow kinetics is not only related to the passive film but also to the p−n junction. Additionally, at 0.75 V, the biggest resistance of charge transfer (R_{ct}) which is related to the obstacle of the p−n junction can be seen from the EIS results in the next section.

The bigger n_0 and smaller $L_{D.eff}$ when tartrate is introduced are attributed to a decrease in the intergranular energy barrier height (E_b) [28]. Tartrate not only increases granular electrical contact by decreasing the insulated S^0 layer between particles due to the affinity of two organic terminals, but also bridges two granules (Fig. 5). Due to the electrostatic effects, tartrate group approaches the surfaces of solids (including covellite-like granule and the LPCCO granule) which are anodic, and its electronic distribution rearrangement occurs due to the changes in the environment (such as electric field, concentration, and temperature), and intermolecular interaction. Additionally, the metal elements on solid surfaces have empty orbitals, which provide affinity for the carboxyl groups of tartrate and conditions for coordination. Both rearrangement and coordination are beneficial for tartrate effectively bridging solid granules, although the position and direction of bridging are related to the surface state of solids. Therefore, the parallel consolidation of passive species is hindered.

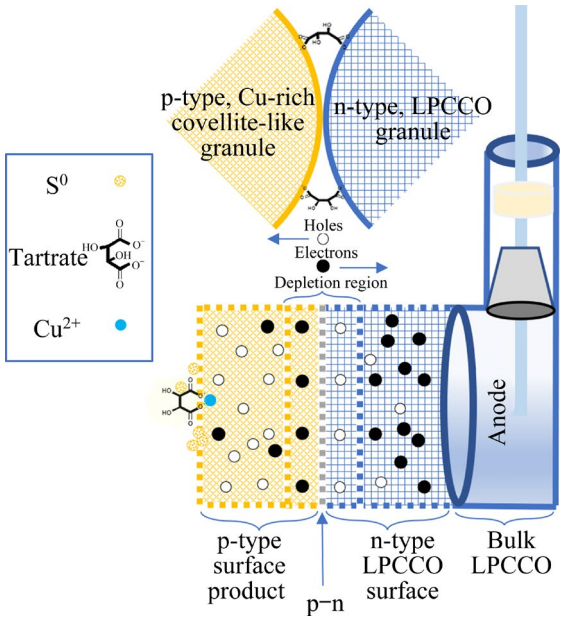

Fig. 5 Description of dissolution of LPCCO in the presence of p−n type semiconductor interface

Vertically, conductive tartrate inserts to the granular domain, thus the barrier height of intergranular hetero-junction or homo-junction decreases. Another electron transfer route via tartrate can be realized by tunneling after the electronic level of tartrate couples with that of two granules. The electron transfer between inter-granular semiconductors facilitated by the organic molecule with a suitable lowest unoccupied molecular

orbital has been reported in the literature [28]. The maximum charge transfer can also be obtained by intimate connections between nanoparticles [29]. Moreover, the increase in the galvanic effect and electron transfer between two sulfides by removing insulating, hydrophobic and impermeable S products and impurities has also been put forward [30,31].

To evaluate the widths (d_{sc}) of the SCR in both cases, Eq. (3) was employed.

$$d_{sc}=2L_{D.eff}\left(\frac{e\Delta\varphi_{sc}}{kT}-1\right) \quad (3)$$

where $\Delta\varphi_{sc}$ is the potential across the SCR [32]. While the value of $\Delta\varphi_{sc}$ is assumed as 0.75 V for both cases, the values of d_{sc} are calculated as 118.8 and 99.0 nm respectively for the cases without and with tartrate, which is in the range of 10−1000 nm reported in the literature [32]. The smaller d_{sc} under the same assumed condition suggests less obstacle for charge carriers when tartrate is present, which may be related to the effect of tartrate on charge carrier density and Debye length.

The negative slope (Fig. 3(a)) at the scope of 0.77−1.24 V indicates that the p-type layer still exists. At the scopes of 0.77−0.97 V and 1.10−1.20 V, the decrease in slope implies an increase in charge carrier density induced by formation of CuS, which is a p-type semiconductor [14]. CuS can be further oxidized to $Cu_{1-x}S$ [33], leading to an increase in slope in the range of 0.97−1.10 V, compared with the slope in the range of 0.77−0.97 V. At higher potential (>1.20 V), intermediate (CuS or $Cu_{1-x}S$) can be oxidized to S^0 or SO_4^{2-} [34], and the downward trend of slope also slows down. When holes are on the way to the surface, they oxidize intermediately to Cu^{2+} [23] that transfers to surface too, subsequently, Cu^{2+} is captured by tartrate (Fig. 5). The complex ion finally enters into bulk solution via electric double layer (EDL). At the scope of 0.52−1.24 V, the smaller value of C^{-2} in the case with tartrate is attributed to the demolition of the passive film [35].

3.2.2 Solid−liquid interface

The surface occupancy (θ) of tartrate adsorbed on LPCCO electrode can be obtained by Eq. (4) [36].

$$\theta=(I_{corr}-I'_{corr})/I_{corr} \quad (4)$$

where I_{corr} and I'_{corr} are the corrosion current in the absence and presence of tartrate, respectively. By fitting Tafel polarization curves (Fig. 3(b)) [34,37], the corrosion currents were obtained, as shown in Table 3. The θ was calculated as 0.295. Additionally, according to Eqs. (5) and (6),

$$\theta/(1-\theta)=K_{ads}C_a \quad (5)$$

$$\Delta G=-2.303RT\cdot\lg(55.5K_{ads}) \quad (6)$$

where R, C_a and 55.5 are the molar gas constant ($J\cdot K^{-1}\cdot mol^{-1}$), concentration of tartrate (g/L), and the concentration of water in the solution (mol/L), respectively, the equilibrium constant (K_{ads}) and Gibbs free energy (ΔG) of the adsorption process were calculated as 0.026 L/g and −92.74 kJ/g, respectively.

When tartrate is present, the smaller anodic Tafel slope (β_a) is observed (Table 3), indicating a faster current increase which continues at the scope of 0.64−0.77 V (b−c region in Fig. 3(b)). Conversely, in the b−c region the current when tartrate is absent only experiences decrease. Additionally, the anodic transfer coefficient (α_a) increases to 0.87 from 0.74 (Table 3), illustrating that tartrate can effectively facilitate the anodic charge/electron transfer across the solid−liquid interface, which is related to the complexation with ions and the attack to passive film [5]. The sum of α_a and α_c exceeds 1 in both cases, indicating the multiple oxidation reactions involving intermediate products [34].

To further study the solid−liquid interface, EIS experiments at different potentials were conducted. According to the four breaks (Points a, b, c and d) labeled in Fig. 3(b), the potentials conducted in EIS were chosen as OCP, OCP+50 mV, OCP+150 mV and OCP+500 mV. As shown in Figs. 6(a−d), for all cases, an incomplete semicircle can be seen at the

Table 3 Kinetics parameters obtained by fitting Tafel curves

Condition	φ_{corr}(vs Ag/AgCl)/V	$I_{corr}/10^{-5}$ A	β_a/(decade·V^{-1})	β_c/(decade·V^{-1})	α_a	α_c
Without tartrate	0.601	1.433	0.0213	0.0112	0.74	1.41
With tartrate	0.612	1.010	0.0182	0.0130	0.87	1.21

φ_{corr}, β_c and α_c are corrosion potential, cathodic Tafel slopes and transfer coefficient, respectively

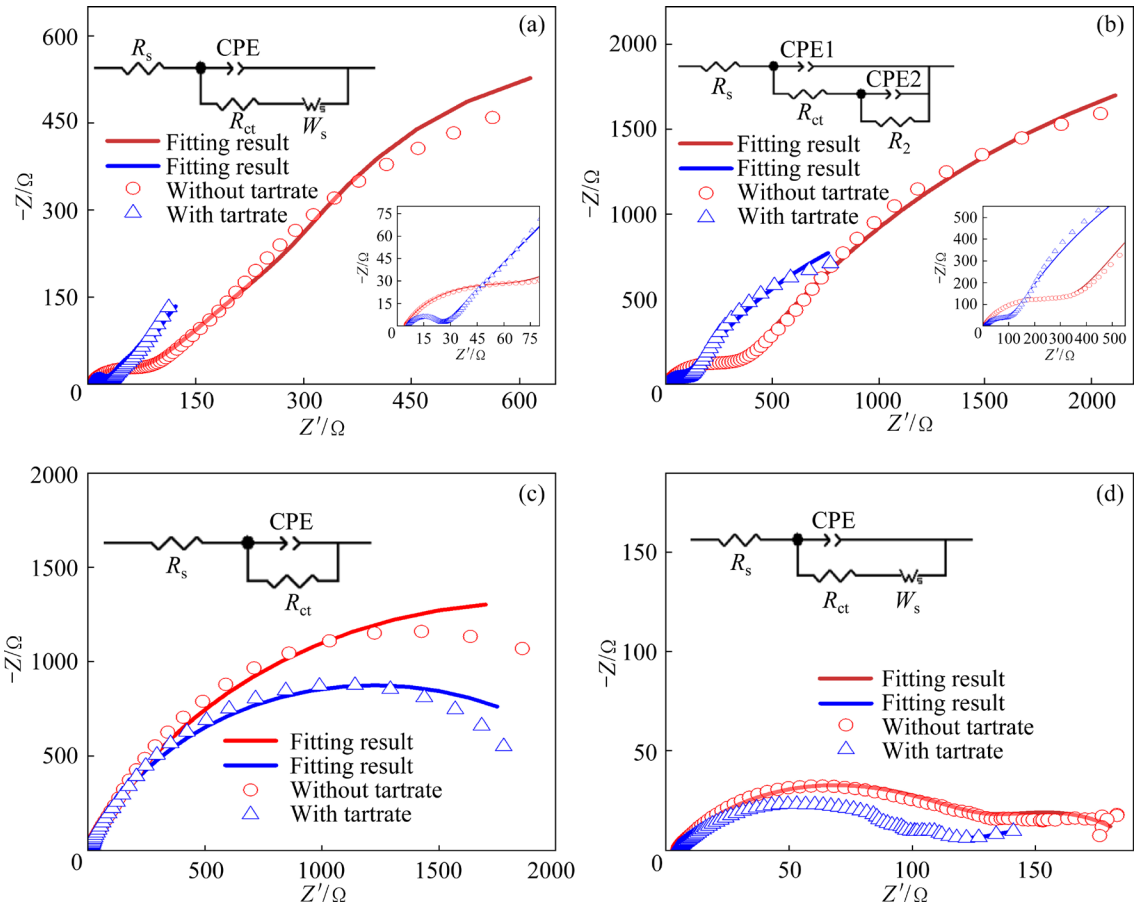

Fig. 6 Nyquist plots in EIS including fitting results by using Randles circuit under different potentials at 318 K: (a) OCP; (b) OCP+50 mV; (c) OCP+150 mV; (d) OCP+500 mV

high-frequency zone, which is attributed to charge transfer (CT) process occurring at the solid−solution interface [38]. At OCP and OCP+500 mV, the low-frequency zone shows a linear behavior (Figs. 6(a) and (d), indicating the diffusion-controlled impedance [35]. By contrast, at OCP+50 mV, the low-frequency zone shows another incomplete semicircle (Fig. 6(b)), which is attributed to CT across the passive film. While at OCP+150 mV (namely about 0.75 V), the low-frequency zone and high-frequency zone jointly constitute the incomplete semicircle (Fig. 6(c)).

By using different Randles circuits (as shown in Figs. 6(a−d)) with constant phase element (CPE), the EIS data was modeled for phase <0° by stepwise fixing values whose errors were less than 10% on ZView software for obtaining interface parameters. There is a good agreement between the experimental and fitting data (Figs. 6(a−d)). The fitting values with errors were presented in Table 4. Here, R_s is the resistance of the solution. R_{ct} and R_2 are the charge transfer resistance of ore oxidation and the resistance of the passive film [3], respectively. The $æ$ (non-ideality of capacitor) and Q (capacitances) are the parameters associated with the CPE. Usually, $æ$ is between 0 to 1. When $æ$ value equals 0.5 or 1, it represents a porous electrode or a pure capacitance, respectively. Q_1 and Q_2 are the double-layer capacitances of the electrode–electrolyte interfaces and passive layer-electrolyte interfaces, respectively. The $Z_{W\text{-}R}$ is the diffusion resistance, and $Z_{W\text{-}P}$ is about 0.5. Here, $Z_{W\text{-}T}$ has a relationship (Eq. (7)) with the effective diffusion thickness (δ) and the diffusion coefficient (D_f) [39].

$$Z_{W\text{-}T}=\delta^2/D_f \quad (7)$$

As shown in Table 4, in both cases, as the increase in potential, the variation of R_{ct} is 'Λ-shaped', namely, it increases, subsequently peaks at OCP+150 mV and finally decreases. This variation is consistent with that in the EIS results of the literature [9]. The increase or decrease in R_{ct}

Table 4 Mode parameters for equivalent circuit of Fig. 6

Condition	R_s/(Ω·cm^2)	Q/(10^{-4} F·cm^{-2})	æ	R_{ct}/(Ω·cm^2)	$Z_{W\text{-}T}$/s	$Z_{W\text{-}P}$	$Z_{W\text{-}R}$/(Ω·cm^2)
OCP	4.82±0.04	0.57±0. 01	0.71±0.01	72.6±0.7	5.20±0.06	0.52±0.01	1252±18
OCP &T	5.54±0.04	0.91±0. 01	0.69±0.01	20.4±0.2	84.75±0.84	0.57±0.01	406±18
OCP+500 mV	4.20±0.04	2.66±0. 02	0.61±0.01	117.7±2.5	10.71±1.01	0.31±0.01	71±5
OCP+500 mV &T	4.30±0.04	11.93±0.10	0.56±0.01	102.8±1.1	12.26±1.39	0.58±0.05	20±2
OCP+150 mV	5.16±0.09	4.37±0.08	0.77±0.01	3809±208	−	−	−
OCP+150 mV &T	5.09±0.09	3.21±0.06	0.77±0.02	2432±75	−	−	−
Condition	R_s/(Ω·cm^2)	Q_1/(10^{-4} F·cm^{-2})	æ$_1$	R_{ct}/(Ω·cm^2)	Q_2/ (10^{-4} F·cm^{-2})	æ$_2$	R_2/(Ω·cm^2)
OCP+50 mV	4.37±0.05	0.33±0.01	0.68±0.01	391.4±5.2	4.08±0.06	0.69±0.01	6784±202
OCP+50 mV &T	5.59±0.39	2.78±0.11	0.57±0.01	139.9±2.9	8.73±0.16	0.76±0.01	3539±179

The case with tartrate is abbreviated as "&T"

with increasing potential is attributed to the formation of the high-resistance passive film [40] or the transpassive dissolution and demolition of film [41], respectively. It is reported that R_{ct} also includes the resistance that a charge carrier overcomes when it crosses the p−n junction [14]. The maximal R_{ct} in this work at OCP+150 mV (about 0.75 V) is related to the obstacle of the p−n junction. A high potential can overcome its resistance, even induce a dielectric breakdown, thus, R_{ct} decreases. While at OCP, because the fewest film is formed on surface, R_{ct} is the lowest. At all potential, after adding tartrate, R_{ct} becomes lower, indicating an easier CT.

The lower æ and æ$_1$ in the case with tartrate indicate severe attacks of the exposed surface and higher surface roughness [35], which also illustrates that tartrate hinders the consolidation of passive species. At OCP and OCP+500 mV, when tartrate is present, the lower $Z_{W\text{-}R}$ indicates an easier diffusion. Additionally, the $Z_{W\text{-}R}$ at OCP+500 mV is much lower than that at OCP, illustrating that a higher applied potential favors diffusion. At OCP+50 mV, R_2 is much bigger than R_{ct}, suggesting a greater impact of passive film on oxidation [42]. When tartrate is present, the lower R_2 demonstrates that the CT across the passive film is easier. This is attributed to the capture and coordination of tartrate's two —COO^- similar to two hands that can grasp metal ions (Fig. 5). When tartrate complex is deported, the organic terminal —CH in tartrate incidentally takes S^0 away by attacking it. Once tartrate complex reaches a certain height, one of —OH resets to its normal position due to the weakening of the electric field, leading to that S^0 is kicked away. The released S^0 is forced to deposit on the unoccupied adjacent position and heap together, therefore, lower æ and æ$_1$ are obtained. The attack to the passive film by organic terminal can open a channel for leaching [43]. While the S^0 insulating layer hinders ET at the solid−liquid interface, which is the rate-limiting step of redox reactions [44]. Additionally, the increase in the accessibility of S^0 to the electrolyte [43] and the decrease in S film [45] could facilitate ET.

The double-layer capacitance (C_{dl}, F) of the electrode can be calculated by Eq. (8). The thickness of passive film (d_p) can be estimated by Eq. (9) [46].

$$\frac{C_{dl}}{A}=\frac{\varepsilon\varepsilon_0}{d} \tag{8}$$

$$\frac{C_p}{A}=\frac{\varepsilon\varepsilon_0}{d_p} \tag{9}$$

where d, C_p and A represent the thickness (m) of the double-layer, the double-layer capacitance (F) of the passive layer−electrolyte interfaces, and the exposed surface area (m^2) of the electrode, respectively. It is worth noting that Q_1 or Q_2 in Table 4 actually stands for the capacitance in per area (F/cm^2) which is equivalent to the term C_{dl}/A or C_p/A, respectively [46]. By using the value of Q_1 or Q_2, and ε [23], d is calculated as 2.17 or 0.26 nm, and d_p is 0.18 or 0.08 nm for the case without or with tartrate respectively. The value of d is in the same order as that (1 nm) reported in the literature, and d_p is smaller than that (1 nm) reported by the literature [46]. The difference is owing to the different leaching systems used. The thinner d_p when tartrate is present can contribute to less

passivation, and fast electron/charge transfer and diffusion through film. Additionally, because of the thinner d, at the same applied potential difference, the electric field intensity of double-layer in the case with tartrate is stronger, which suggests a faster reaction rate.

3.2.3 Interface diffusion

Interface diffusion is commonly considered to have a significant effect on reaction rate [46]. Here, based on Eq. (7), the value of diffusion thickness (δ) can be obtained if diffusion coefficient (D_f) is known. Moreover, D_f can be calculated by the Randles−Sevcik equation as

$$J=0.4463z^{1.5}F^{1.5}D_f^{0.5}C_iR^{-0.5}T^{-0.5}v^{0.5} \quad (10)$$

where J, z, F, and C_i are the peak current density (A/m^2), electron number of reaction, Faraday constant (C/mol), and concentration of oxidant (mol/L), respectively. Consequently, to obtain D_f, the LSV experiments were performed at different scanning rates (v, V/s). As shown in Fig. 7, in both cases, at the potential around 0.75 V, the current is feeble. A main anodic peak at the scope of 0.8−1.2 V is observed, which is attributed to the formation of CuS [47,48], as

$$2CuFeS_2-8e=CuS+Cu^{2+}+2Fe^{2+}+3S^0 \quad (11)$$

Figure 7 shows that the peak potential (φ_p) shifts positively as v increases, which is attributed to that the bigger v leads to severer concentration polarization caused by untimely diffusion, implying that the diffusion is closely relative to dissolution reaction. The increase of current with the increase in v may be attributed to the increase in current of EDL. Compared with φ_p and I_p (peak current) in the case without tartrate at scanning rate of 0.5 mV/s (the LSV curve at lower v can be used to more representatively analyze the passivation and dissolution [13]), the lower φ_p and higher I_p in the case with tartrate indicate an easier and faster oxidation reaction.

By using the slopes in the inserts of Fig. 7, the values of D_f were calculated as 5.5×10^{-11} and 24.8×10^{-11} m^2/s for the cases without and with tartrate, respectively. The big D_f indicates that tartrate can facilitate species diffusion. Combining D_f with $Z_{W\text{-}T}$ at OCP+500 mV in Table 4, the δ was calculated as 24.3 and 55.1 μm for the cases without and with tartrate, respectively. The big δ when tartrate is present is due to the adsorption on surface.

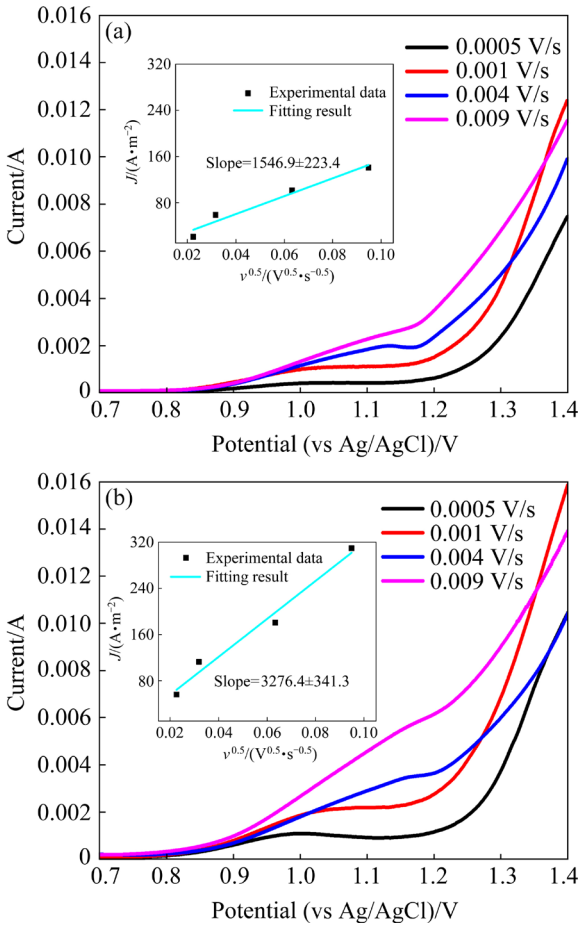

Fig. 7 LSV curves at different v without (a) and with (b) tartrate at 318 K (The insert shows the plot of J versus $v^{0.5}$ and corresponding fitting results and linear slopes)

3.2.4 Apparent activation energy of interface reaction

The apparent activation energy (E_a) of interface reaction is one of the most important parameters in electrochemical kinetic, which can be described by the Arrhenius equation (Eq. (12)):

$$\lg k_a=\lg A_a-\frac{E_a}{2.303RT} \quad (12)$$

where k_a and A_a are the apparent reaction rate constant and pre-exponential factor, respectively.

As shown in Fig. 8, in both cases, the peaks in LSV at the scope of 0.8−1.2 V are attributed to the interface Reaction (11) [47,48]. The φ_p shifts negatively with the increase in temperature and the addition of tartrate at the same temperature, indicating that these operations make interface reaction easier. Additionally, I_p increases with the increase in temperature, suggesting that heating can promote reaction rate. When lg$J$ was plotted against

T^{-1}, a linear relationship was obtained, as shown in the insert of Fig. 8. Therefore, the value of E_a (namely, 'pseudo' activation energies [49]) was calculated as 48.1 and 28.4 kJ/mol, respectively for the cases without and with tartrate. The lower E_a in the case with tartrate illustrates a lower threshold for interface reaction.

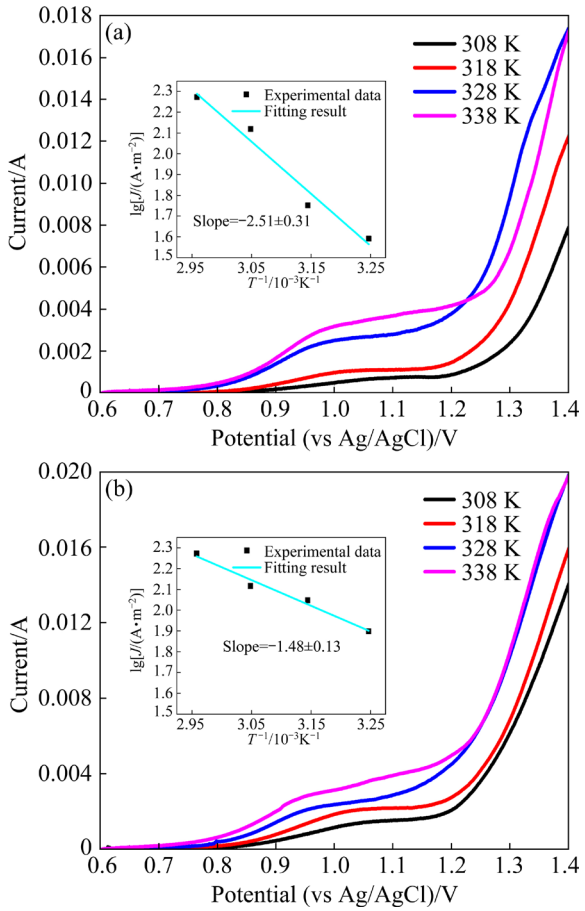

Fig. 8 LSV curves at different T without (a) and with (b) tartrate (v=1 mV/s) (The insert shows the plot of lg J versus T^{-1} and corresponding fitting results and linear slopes)

According to the above experiments, the energy process involving E_a of interface reaction is put forward. As shown in Fig. 9, the Point A is the lowest energy state of the reactants ([Reactants]). In the case without tartrate, the reaction process initials from Point A, via the Point C which is the activation energy barrier (namely E_a), and finally reaches the lowest energy state (Point D) of products ([Products], red line in Fig. 9), assuming that Reaction 11 is exothermic. When tartrate is present, due to the coordination of tartrate to metal ions around electrode surface, ions become more stable and the energy of products state becomes lower ([Products]′, blue dot line in Fig. 9), leading to that E_a decreases to E_a'. The lower E_a' is more favorable to interface reaction. As a result, the interface reaction process changes to D' via C'. The greater stability of product (e.g. copper complex) determining a higher leaching rate has been confirmed [50].

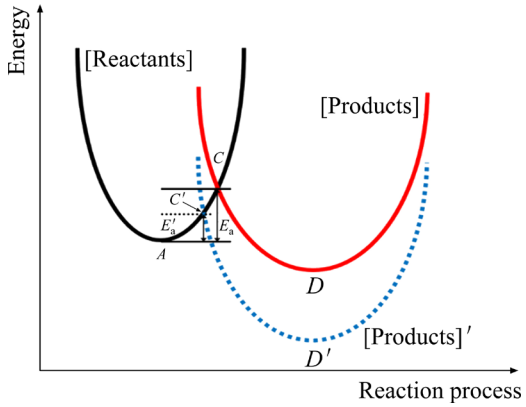

Fig. 9 Energy process involved E_a of interface reaction without (solid line) and with (dot line) tartrate

4 Conclusions

(1) M−S plot indicates that LPCCO is an n-type semiconductor which produces a p-type copper-rich, covellite-like layer (e.g. CuS) during leaching, leading to the formation of a p−n junction on the surface that hinders electron transfer and makes R_{ct} reach the maximum at 0.75 V. When tartrate is present, the bigger n_0, and smaller $L_{D.eff}$ and d_{sc} are obtained.

(2) Tafel polarization result presents a lower β_a and higher α_a, illustrating that tartrate can effectively facilitate anodic charge/electron transfer across solid−liquid interface. The results of EIS at different potentials based on the four breaks in the Tafel curve reveal a lower $æ$, $æ_1$, $Z_{W\text{-}R}$, R_{ct}, and R_2 with tartrate, indicating rougher surfaces, and the improvement of interface diffusion, favorable CT of LPCCO oxidation and CT across passive film, respectively. The thinner d and d_p after addition of tartrate illustrate a stronger electric field intensity of double-layer and a less passivation effect, respectively.

(3) By combining the results of EIS and LSV experiments, the favorable effect of tartrate on interface diffusion is also verified by a big D_f. The lower E_a' implies a lower threshold for interface reaction after adding tartrate. These favorable

changes in interface properties resulting from the addition of tartrate improved Cu extraction from LPCCO.

CRediT authorship contribution statement

Xin-Jie LIU: Investigation, Methodology, Software, Fitting, Formal analysis, Validation, Data curation, Writing – Original draft, Writing – Review and editing, Visualization; **Ya-long LIAO:** Resources, Supervision, Formulation of research ideas, Project administration, Paper modification and editing; **Qing-feng LIU** and **Min WU:** Writing – Review & editing.

Declaration of competing interest

The authors declare that they have no known competing financial interests or personal relationships that could have appeared to influence the work reported in this paper.

Acknowledgments

This work was supported by the National Natural Science Foundation of China (No. 21978122).

References

[1] TIAN Zu-yuan, LI Hao-dong, WEI qian, QIN Wen-qiang, YANG Cong-ren. Effects of redox potential on chalcopyrite leaching: An overview [J]. Minerals Engineering, 2021, 172: 107135.

[2] GHAHREMANINEZHAD A, ASSELIN E, DIXON D G. Electrochemical evaluation of the surface of chalcopyrite during dissolution in sulfuric acid solution [J]. Electrochimica Acta, 2010, 55: 5041−5056.

[3] BAI Yun-long, WANG Wei, DONG Kai-wei, XIE Feng, LU Dian-kun, CHANG Yong-feng, JIANG Kai-xi. Effect of microwave pretreatment on chalcopyrite dissolution in acid solution [J]. Journal of Materials Research and Technology, 2022, 16: 471−481.

[4] XI Jia-jun, LIAO Ya-long, JI Guang-xiong, LIU Qing-feng, WU Yue. Mineralogical characteristics and oxygen pressure acid leaching of low-grade polymetallic complex chalcopyrite [J]. Journal of Sustainable Metallurgy, 2022, 8: 1628−1638.

[5] BARRERA-MENDOZA G E, LAPIDUS G T. The effect of chemical additives on the electro-assisted reductive pretreatment of chalcopyrite [J]. Hydrometallurgy, 2015, 158: 35−41.

[6] ABDELRAHEEM M T O, AGACAYAK T. Effect of organic and inorganic compounds on dissolution kinetics of chalcopyrite in hydrogen peroxide−Hydrochloric acid system [J]. Journal of Saudi Chemical Society, 2022, 26: 101478.

[7] NAZARI G, DIXON D G, DREISINGER D B. The role of silver-enhanced pyrite in enhancing the electrical conductivity of sulfur product layer during chalcopyrite leaching in the Galvanox™ process [J]. Hydrometallurgy, 2012, 113: 177−184.

[8] TANNE C, SCHIPPERS A. Electrochemical investigation of microbially and galvanically leached chalcopyrite [J]. Hydrometallurgy, 2021, 202: 105603.

[9] CASTILLO-MAGALLANES N, CRUZ R, LÁZARO I. Effect of organic agents on the oxidation process of chalcopyrite in a sulfuric acid solution [J]. Electrochimica Acta, 2020, 355: 136789.

[10] AL-ZUBEIDI A, GODFREY D, ALBRECHT T. Disentangling chemical effects in ionic-liquid-based Cu leaching from chalcopyrite [J]. Journal of Electroanalytical Chemistry, 2018, 819: 130−135.

[11] WANG Yu-yang, GU Jian-kang, ZHANG Bo-hai, LI Guo-ran, LIU Sheng, GAO Xue-ping. Specific adsorption reinforced interface enabling stable lithium metal electrode [J]. Advanced Functional Materials, 2022, 32: 2112005.

[12] CRUNDWELL F K. The semiconductor mechanism of dissolution and the pseudo-passivation of chalcopyrite [J]. Canadian Metallurgical Quarterly, 2015, 54: 279−288.

[13] DEBERNARDI G, CARLESI C. Chemical-electrochemical approaches to the study passivation of chalcopyrite [J]. Mineral Processing and Extractive Metallurgy Review, 2013, 34: 10−41.

[14] REN Zi-he, CHAO Chi-wei, KRISHNAMOORTHY P, ASSELIN E, DIXON D G, MORA N. The overlooked mechanism of chalcopyrite passivation [J]. Acta Materialia, 2022, 236: 118111.

[15] HE Li-po, SUN Shu-ying, MU Yan-yu, SONG Xing-fu, YU Jing-guo. Recovery of lithium, nickel, cobalt, and manganese from spent lithium-ion batteries using l-tartaric acid as a leachant [J]. ACS Sustainable Chemistry & Engineering, 2017, 5: 714−721.

[16] LALLEMAND C, AMBROSI J P, BORSCHNECK D, ANGELETTI B, CHAURAND P, CAMPOS A, DESMAU M, FEHLAUER T, AUFFAN M, LABILLE J, ROCHE N, POIZAT L, COLLIN B, ROSE J, LEVARD C. Potential of ligand-promoted dissolution at mild pH for the selective recovery of rare earth elements in bauxite residues [J]. ACS Sustainable Chemistry & Engineering, 2022, 10: 6942−6951.

[17] YLINIEMI J. Surface layer alteration of multi-oxide silicate glasses at a near-neutral pH in the presence of citric and tartaric acid [J]. Langmuir, 2022, 38: 987−1000.

[18] CHEN Jun-nan, XIE Feng, WANG Wei, FU yan, WANG Jian. Leaching of gold and silver from a complex sulfide concentrate in copper-tartrate-thiosulfate solutions [J]. Metals, 2022, 12: 1152.

[19] YE Long-gang, DUAN Liang-hong, LIU Wei, HU Yu-jie, OUYANG Zhen, YANG Sheng-hai, XIA Zhi-mei. Facile method for preparing a nano lead powder by vacuum decomposition from spent lead-acid battery paste: leaching and desulfuration in tartaric acid and sodium tartrate mixed lixivium [J]. Hydrometallurgy, 2020, 197: 105450.

[20] KURSUNOGLU S, TOP S, KAYA M. Recovery of zinc and lead from Yahyali non-sulphide flotation tailing by sequential acidic and sodium hydroxide leaching in the presence of potassium sodium tartrate [J]. Transactions of Nonferrous Metals Society of China, 2020, 30: 3367−3378.

[21] CHEN Jun-nan, XIE Feng, WANG Wei, FU Yan, WANG Jian. Leaching of a carbonaceous gold concentrate in copper−tartrate−thiosulfate solutions [J]. Minerals Engineering, 2022, 183: 107605.

[22] GHAHREMANINEZHAD A, RADZINSKI R, GHEORGHIU T, DIXON D G, ASSELIN E. A model for silver ion catalysis of chalcopyrite ($CuFeS_2$) dissolution [J]. Hydrometallurgy, 2015, 155: 95−104.

[23] CRUNDWELL F K, von ASWEGEN A, BRYSON L J, BILEY C, CRAIG D, MARSICANO V D, KEARTLAND J M. The effect of visible light on the dissolution of natural chalcopyrite ($CuFeS_2$) in sulphuric acid solutions [J]. Hydrometallurgy, 2015, 158:119−131.

[24] WANG Chong-mou, MALLOUK T E. Wide-range tuning of the titanium dioxide flat-band potential by adsorption of fluoride and hydrofluoric acid [J]. The Journal of Physical Chemistry, 1990, 94: 4276−4280.

[25] NICOL M J, ZHANG Su-chun. Anodic oxidation of iron(II) and copper(I) on various sulfide minerals in chloride solutions [J]. Hydrometallurgy, 2016, 166: 167−173.

[26] DEBNATH K, MAJUMDER T, MONDAL S P. Photoelectrochemical study of hydrothermally grown vertically aligned rutile TiO_2 nanorods [J]. Chemical Physics, 2022, 561: 111609.

[27] ZHAO Hong-bo, HU Ming-hao, LI Yi-ni, ZHU Shan, QIN Wen-qing, QIU Guan-zhou, WANG Jun. Comparison of electrochemical dissolution of chalcopyrite and bornite in acid culture medium [J]. Transactions of Nonferrous Metals Society of China, 2015, 25: 303−313.

[28] GAMON J, GIAUME D, LEFÈVRE G, LE MERCIER T, BARBOUX P. The effect of organic additives on the intergranular conductivity of Al-doped ZnO [J]. RSC Advances, 2017, 7: 38019−38027.

[29] LI Gong-hu, GRAY K A. The solid-solid interface: Explaining the high and unique photocatalytic reactivity of TiO_2-based nanocomposite materials [J]. Chemical Physics, 2007, 339: 173−187.

[30] AHMADI A, RANJBAR M, SCHAFFIE M. Catalytic effect of pyrite on the leaching of chalcopyrite concentrates in chemical, biological and electrobiochemical systems [J]. Minerals Engineering, 2012, 34: 11−18.

[31] LI Lin, GHAHREMAN, A. The synergistic effect of Cu^{2+}–Fe^{2+}–Fe^{3+} acidic system on the oxidation kinetics of Ag-doped pyrite [J]. The Journal of Physical Chemistry C, 2018, 122: 26897−26909.

[32] O'CONNOR G M, EKSTEEN J J. A critical review of the passivation and semiconductor mechanisms of chalcopyrite leaching [J]. Minerals Engineering, 2020, 154: 106401.

[33] BAI Yun-long, WANG Wei, XIE Feng, LU Dian-kun, JIANG Kai-xi, DREISINGER D. In-situ electrochemical study of chalcopyrite pressure oxidation leaching from 110 °C to 150 °C under saturated vapor pressure [J]. Arabian Journal of Chemistry, 2022, 15: 104139.

[34] LI Lin, SOLEYMANI M, GHAHREMAN A. New insights on the role of lattice-substituted silver in catalytic oxidation of chalcopyrite [J]. Electrochimica Acta, 2021, 369: 137652.

[35] RAFSANJANI-ABBASI A, DAVOODI A. Electrochemical characterization of natural chalcopyrite dissolution in sulfuric acid solution in presence of peroxydisulfate [J]. Electrochimica Acta, 2016, 212: 921−928.

[36] HALEEM S, WANEES S, AAL E, FAROUK A. Factors affecting the corrosion behaviour of aluminium in acid solutions. I. Nitrogen and/or sulphur-containing organic compounds as corrosion inhibitors for Al in HCl solutions [J]. Corrosion Science, 2013, 68: 1−13.

[37] YANG Cong-ren, QIN Wen-qing, ZHAO Hong-bo, WANG Jun, WANG Xing-jie. Mixed potential plays a key role in leaching of chalcopyrite: Experimental and theoretical analysis [J]. Industrial & Engineering Chemistry Research, 2018, 57: 1733−1744.

[38] ARENA F A, SUEGAMA P H, BEVILAQUA D, DOS SANTOS A L A, FUGIVARA C S, BENEDETTI A V. Simulating the main stages of chalcopyrite leaching and bioleaching in ferrous ions solution: An electrochemical impedance study with a modified carbon paste electrode [J]. Minerals Engineering, 2016, 92: 229−241.

[39] FERNÁNDEZ M L, PETROVA M, HAUFFMAN T, MUSELLE T, DONEUX T, HUBIN A. A study of the electron transfer inhibition on a charged self-assembled monolayer modified gold electrode by odd random phase multisine electrochemical impedance spectroscopy [J]. Electrochimica Acta, 2014, 140: 266−274.

[40] HIROYOSHI N, KUROIWA S, MIKI H, TSUNEKAWA M, HIRAJIMA T. Synergistic effect of cupric and ferrous ions on active-passive behavior in anodic dissolution of chalcopyrite in sulfuric acid solutions [J]. Hydrometallurgy, 2004, 74: 103−116.

[41] LI lin, BERGERON I, GHAHREMAN A. The effect of temperature on the kinetics of the ferric-ferrous redox couple on pyrite [J]. Electrochimica Acta, 2017, 245: 814−828.

[42] BAI Yun-long, WANG Wei, XIE Feng, LU Dian-kun, JIANG Kai-xi. Effect of temperature, oxygen partial pressure and calcium lignosulphonate on chalcopyrite dissolution in sulfuric acid solution [J]. Transactions of Nonferrous Metals Society of China, 2022, 32: 1650−1663.

[43] ZHANG Hao, WEI De-zhou, LIU Wen-gang, HOU Duan-xu, ZHANG Rui-yang. Enhancement mechanism of polyoxyethylene nonyl phenyl ether on the bioleaching of chalcopyrite [J]. Minerals Engineering, 2021, 173: 107237.

[44] ZHAO Hong-bo, ZHANG Yi-sheng, ZHANG Xian, QIAN Lu, SUN Meng-lin, YANG Yu, ZHANG Yan-sheng, WANG Jun, KIM H, QIU Guan-zhou. The dissolution and passivation mechanism of chalcopyrite in bioleaching: An overview [J]. Minerals Engineering, 2019, 136: 140−154.

[45] KUZMINA O, SYMIANAKIS E, GODFREY D, ALBRECHT T, WELTON T. Ionic liquids for metal extraction from chalcopyrite: solid, liquid and gas phase studies [J]. Physical Chemistry Chemical Physics, 2017, 19: 21556−21564.

[46] GHAHREMANINEZHAD A, DIXON D G, ASSELIN E. Kinetics of the ferric-ferrous couple on anodically passivated chalcopyrite ($CuFeS_2$) electrodes [J]. Hydrometallurgy, 2012, 125: 42−49.

[47] BAI Yun-long, WANG Wei, ZHAO Shang-rong, LU Dian-kun, XIE Feng, DREISINGER D. Effect of mechanical activation on leaching behavior and mechanism of

chalcopyrite [J]. Mineral Processing and Extractive Metallurgy Review, 2022, 43: 440−452.
[48] ZENG Wei-ming, QIU Guan-zhou, ZHOU Hong-bo, CHEN Miao. Electrochemical behaviour of massive chalcopyrite electrodes bioleached by moderately thermophilic microorganisms at 48 °C [J]. Hydrometallurgy, 2011, 105: 259−263.
[49] MINEY P G, CUNNANE V J. A study of the passivation peak current density for (100) oriented silicon in tetramethylammonium hydroxide (TMAH): Effect of temperature, concentration and carrier type [J]. Electrochimica Acta, 2004, 49: 1009−1018.
[50] NURTAZINA N, UVAROV N, AZHIGULOVA R, TYAPKIN P. Chalcopyrite leaching by amino acid solutions in the presence of hydrogen peroxide [J]. Physicochemical Problems of Mineral Processing, 2022, 58: 157067.

酒石酸钠对低品位多金属复杂黄铜矿浸出界面的影响

刘新杰，廖亚龙，刘庆丰，武 敏

昆明理工大学 冶金与能源工程学院，昆明 650093

摘 要：通过添加酒石酸钠，提高低品位多金属复杂黄铜矿(LPCCO)在酸性铁电解液中铜的浸出率。利用电化学方法系统研究酒石酸钠对浸出反应界面的影响。Mott−Schottky 实验结果表明，无论是否添加酒石酸钠，初始的 n 型 LPCCO 表面都会转变为具有严重阻碍电荷转移的 p−n 结的表面。添加酒石酸钠后，因酒石酸根桥接半导体颗粒降低了晶间能垒高度，获得了更小的 Debye 长度和更高的电荷载流子密度；结合 Tafel 和 LSV 分析的 EIS 结果表明，加入酒石酸钠后反应界面转变为更薄的钝化膜和电双层，具有较大的扩散系数，从而降低了浸出反应的表观活化能，这些界面性质促进了 LPCCO 的溶解。

关键词：界面；黄铜矿；钝化；半导体；浸出

(Edited by Xiang-qun LI)